Quantum Monte Carlo treatment of elastic exciton-exciton scattering

J. Shumway* and D. M. Ceperley
Department of Physics and the National Center for Supercomputing Applications, University of Illinois at Urbana-Champaign, 1110 West Green Street, Urbana, Illinois 61801

(Received 21 July 1999; revised manuscript received 20 November 2000; published 5 April 2001)

We calculate cross sections for low energy, elastic, bulk, *s*-wave exciton-exciton scattering within the single-band effective mass approximation. Unlike previous theoretical approaches, we give a complete, nonperturbative treatment of the four-particle scattering problem. Diffusion Monte Carlo is used to calculate the essentially exact energies of scattering states, from which phase shifts are determined. For the case of equal-mass electrons and holes, which is equivalent to positronium-positronium scattering, we find $a_s = 2.1a_x$ for scattering of singlet excitons and $a_s = 1.5a_x$ for triplet excitons, where a_x is the excitonic radius. The spin dependence of the cross sections arises from the spatial exchange symmetry of the scattering wave functions. A significant triplet-triplet to singlet-singlet scattering process is found, which is similar to the reported effects in recent experiments and theory for excitons in quantum wells. We also show that the scattering length can change sign and diverge for some values of the mass ratio m_h/m_e, an effect not seen in previous perturbative treatments.

DOI: 10.1103/PhysRevB.63.165209 PACS number(s): 71.35.Cc, 36.10.Dr

I. INTRODUCTION

Excitons in semiconductors have been the subject of many experimental and theoretical investigations of Bose condensation. Low-energy exciton-exciton interactions are characterized by the exciton-exciton scattering length a_s that determines the thermodynamics of a low-density gas and is crucial for modeling the thermalization time of a dilute exciton gas. Despite its importance, the exciton-exciton scattering length is an elusive quantity, being difficult to measure experimentally or to estimate theoretically.

As is well known in atomic physics, scattering lengths can be extremely sensitive to the details of the interactions between particles. In particular, the existence of a weakly bound or nearly bound state causes the scatter length to become quite large. Therefore, *a priori* one should suspect that exciton-exciton scattering may be a very material dependent property of semiconductors. Reliable theoretical predictions of exciton-exciton scattering lengths require both a very accurate Hamiltonian for the semiconductor and an accurate solution to the (four-particle) scattering problem. In this paper we provide an essentially exact solution to bulk, *s*-wave exciton-exciton scattering for a commonly used single-band effective mass Hamiltonian. This solution allows us to study three important questions: (1) how sensitive is the scattering length to the mass ratio m_e/m_h, (2) how does the scattering length depend on spin states (singlet or triplet) of the scattering excitons, and (3) to what degree can interexciton exchange of electrons or holes cause excitons to scatter into different spin states? This calculation also serves as a benchmark for the single-band limit of more complicated scattering Hamiltonians. We discuss possible extensions of this method to non-*s*-wave scattering, treatment of multiband models, and applications to heterostructures in the Conclusion.

One experimental method for measuring the exciton scattering cross section is to look at linewidth broadening of the recombination spectra in a gas of excitons. Collisions between excitons increase the linewidth, causing the linewidth to depend on the exciton-exciton scattering rate $n\sigma v$, where n is the density and v is a typical exciton velocity. Extracting cross sections from a linewidth requires that (1) the density and velocity distribution are known, and (2) elastic scattering is the fastest process. As discussed below, Cu_2O is a good material for comparison to the model studied in this work. Snoke *et al.*[1,2] have performed such experiments on Cu_2O and have found a linewidth broadening that suggests an upper bound of $4a_x$ on the scattering length. Although our simulations do not exactly model Cu_2O, we will compare our results to this value.

II. THEORETICAL BACKGROUND

Theoretical approaches to this problem start with the effective-mass approximation, in which the system under consideration consists of two electrons, labeled 1 and 2, and two holes, labeled a and b. The Hamiltonian is

$$H = -\lambda_1\nabla_1^2 - \lambda_2\nabla_2^2 - \lambda_a\nabla_a^2 - \lambda_b\nabla_b^2 - r_{a1}^{-1} - r_{b2}^{-1} - r_{a2}^{-1} - r_{b1}^{-1} + r_{12}^{-1} + r_{ab}^{-1}, \quad (1)$$

where $\lambda = \hbar^2/2m$. The Hamiltonian has symmetry under exchange of electrons and exchange of holes, so eigenstates may be denoted by two exchange quantum numbers. The *s*-wave states are symmetric under exchange of excitons; a condition which is satisfied by states ϕ^{++} and ϕ^{--}, where the $+$ $(-)$ signs refer to (anti)symmetry under exchange of electrons and holes, respectively. (States ϕ^{+-} and ϕ^{-+} are *p*-wave states.) Although this Hamiltonian is a well-accepted model for exciton-exciton scattering, we should point out a few of its deficiencies. For small excitons, such as those in Cu_2O, that have radii not much larger than the lattice spacing, nonparabolic terms in the kinetic energy and other corrections to the potential energy may be necessary. For many semiconductors, such as Si, Ge and $In_{1-x}Ga_xAs$, the valence band is a mixture of three bands and cannot be described by

a single parabolic band. That is, the valence band edge is fourfold degenerate with $j=3/2$, and the spin-orbit split-off band with $j=1/2$ is lower in energy. Possible extensions of this method to multi-band Hamiltonians is discussed in the Conculsion. In the case of Cu_2O, the band order is reversed. The valence band is the parabolic spin-orbit split-off band with $j=1/2$, and the holes may be described by the single band Hamiltonian. Interband exchange (virtual electron-hole recombination) is an important effect that has been neglected and could be modeled by an additional spin-dependent potential term.

This Hamiltonian also describes a family of scattering processes for other particles, including hydrogen-hydrogen, positronium-positronium, and muonium-muonium scattering. The equal mass case is at an extreme (positronium scattering), where the Born-Oppenheimer approximation is the least applicable.

There have been several theoretical estimates of exciton-exciton scattering for bulk systems[3–5] and quantum wells[6,7] as well as calculations on biexciton-biexciton scattering,[8] Only the bulk, elastic scattering calculations[3,4] are directly comparable to the results of this paper, but the techniques presented here could be generalized to the other scattering problems. Also, the results presented here provide a benchmark for evaluating the approximations used in other theoretical treatments and could lend insight into the reliability of the approximations in more complicated situations.

One standard theoretical approach is diagrammatic perturbation theory as presented in the work of Keldysh and Kozlov[9] and Haug and Hanamura.[10] They estimated the exciton-exciton scattering matrix as arising from a single term $\langle k_1+q,k_2-q|H_{\rm int}|k_1,k_2\rangle$, where $|k_1,k_2\rangle$ represents a state of two noninteracting excitons with momentum k_1 and k_2 and $H_{\rm int}$ is the interexciton Coulomb interaction. This method gives an estimate of $a_s=\frac{13}{6}a_x$ (independent of the mass ratio), where $a_x=m_e^{-1}+m_h^{-1}$ is the exciton radius, but it is an uncontrolled approximation that may have limited validity in the low energy limit. One serious drawback of the method is that it does not include effects of the biexciton in the scattering. As we show later, biexciton vibrational states cause strong dependence of the scattering length on the mass ratio m_e/m_h, which is not captured by the low order perturbation theory.

A second common approach was developed by Elkomoss and Munschy.[4] It uses an effective exciton-exciton potential defined by $V_{\rm eff}(R)=\langle\phi_f(R)|H|\phi_f(R)\rangle$, where $\phi_f(R)$ is the wave function for two free excitons a distance R apart. The effective potential $V_{\rm eff}$ arises from the Hartree term and is used in a two-particle central-field calculation. While an exciton-exciton scattering pseudo-potential would be a very useful tool, this approximate form has some serious drawbacks. Among its deficiencies are; a lack of correlation, no van der Waals attraction, a failure to reproduce biexciton states, and a vanishing interaction potential for $m_e=m_h$. The cross sections calculated by this method are small and lack qualitative agreement with the results of the present work.

Some insight into exciton-exciton scattering can be gained by considering the bound states, biexcitons. Since the number of bound states $N_{\rm B}$ enters in the phase shift at zero energy $\delta(0)=\pi N_{\rm B}$, it is necessary that a good computation method for low energy scattering be able to accurately calculate biexciton binding energies.[11] For the mass ratios considered (and far beyond, including deuterium), the biexcitons cannot bind in the ϕ^{--} states, so biexcitons in rotational s states always have ϕ^{++} wave functions. Detailed theoretical descriptions of biexcitons can be found in Ref. 12. The equal mass case was shown to have a bound biexciton by Hyllerass and Ore using a variational argument,[13] and a better variational estimate of the binding energy was given by Brinkman, Rice, and Bell,[14] who found $E_{\rm B}=0.029E_x$, where $E_x=0.5/(m_e^{-1}+m_h^{-1})$ is the exciton binding energy. However, because of the importance of correlation energy, the latter variational treatment was missing *half* of the biexciton binding energy, as shown by diffusion Monte Carlo (DMC) calculations,[15,16] which find $E_{\rm B}=0.064\,04(4)E_x$. DMC is a quantum Monte Carlo (QMC) method that uses a random walk to project out the ground state wave function from a variational wave function, in order to stochastically sample the exact ground state energy. The success of DMC for calculating biexciton energies has been a motivation for its use in the present scattering calculations.

III. METHOD: QUANTUM MONTE CARLO CALCULATION OF SCATTERING

A. *R*-matrix approach and scattering boundary conditions

The R-matrix approach to scattering is to examine the standing waves of the system. As shown by Carlson, Pandharipande, and Wiringa[17] and Alhassid and Koonin,[18] by fixing nodes in the standing waves the scattering problem may be cast as a ground state problem suitable for QMC methods. For an elastic scattering process, we label the distance between the products by R and the reduced mass of the products by m_r. In exciton-exciton scattering there is a subtlety in the definition of R due to interexciton exchange, which we will address below in our discussion of the exciton-exciton scattering wave functions. Nonetheless, for large separation R, the relative motion of the products is free-particle-like, so the many-body wave function depends on R as

$$\phi\propto\sin[kR-\tfrac{1}{2}l\pi+\delta_l(k)], \tag{2}$$

where l is the relative angular momentum, k is the scattering momentum, and $\delta_l(k)$ is the phase shift. If we constrain the wave function to have a node at a large exciton separation R_n, we find a discrete energy spectrum $E_\alpha(R_n)$, which may be computed by ground state or excited state methods, such as DMC. Each choice of R_n gives a spectrum of states $\phi_a,\alpha=1,2,\ldots$, with energies E_α that determine values of $\delta_l(k)$,

$$\delta_l(k_\alpha)=-k_\alpha R_n+\tfrac{1}{2}l\pi+\alpha\pi, \tag{3}$$

where $k_\alpha=\sqrt{2m_rE_\alpha}$. The scattering matrix elements are determined by the phase shifts,

$$S_l(k)=\frac{1}{2ik}\exp[2i\delta_l(k)]-1. \tag{4}$$

Carlson and Shiavilla have also proposed fixing the logarithmic derivative of the wave function at the boundary instead of setting wave function to zero,[19]

$$\left.\frac{\hat{S}\cdot\nabla_R\phi}{\phi}\right|_{R=R_b}=\beta, \tag{5}$$

where $\hat{S}$ is the normal to the boundary surface, at a fixed radius R_b, and β parametrizes the boundary condition. This formulation has the advantage separating the choice of simulation size R_b (subject to R_b lying in the asymptotic region) from the sampling of energy, which is handled by varying β and is particularly well suited for finding the scattering length. The application to variational Monte Carlo (VMC) calculations is straightforward, but preserving the boundary condition in DMC calculations requires a method of images.[20] The results presented here do not use the logarithmic-derivative boundary condition.

B. Calculation of excited states

The use of excited states $\phi_\alpha(\alpha>1)$ is necessary when there is a bound state and, more generally, when the scattering state being studied has its first node before the asymptotic region is reached. We use a QMC method to calculate excited states developed by Ceperley and Bernu,[21] to adapt VMC and DMC methods for a Hilbert space of several low energy wave functions. A set of m trial wave functions is chosen f_α, where $\alpha=1,\ldots,m$. The generalized eigenvalue equation to be solved is[21]

$$\sum_{\beta=1}^{m}[H_{\alpha\beta}(t)-\Lambda_k(t)N_{\alpha\beta}]d_{k\beta}(t)=0, \tag{6}$$

where $d_k(t)$ is the kth eigenvector with eigenvalue $\Lambda_k(t)$ and the matrices N and H are the overlap and Hamiltonian matrices in our trial basis, given by

$$N_{\alpha\beta}(t)=\int dR_1dR_2f_\alpha^*(R_2)e^{-tH}f_\beta(R_1), \tag{7}$$

$$H_{\alpha\beta}(t)=\int dR_1dR_2Hf_\alpha^*(R_2)e^{-tH}f_\beta(R_1). \tag{8}$$

The parameter t is the projection time. The eigenvalues $\Lambda_k(t)$ are energy eigenvalues E_k within the Hilbert space spanned by the projected trial functions $\{e^{-tH/2}f_\alpha\}$, and approach the exact energy eigenvalues in the limit of large t.

The matrices N and H are sampled with random walks, using a guiding function ψ that must be positive everywhere. The guiding function must have significant overlap with all basis functions and should be optimized to decrease the variance of the sampled matrices. At each step $i+1$ in the random walk, the coordinates R_{i+1} of the particles are updated using

$$R_{i+1}=R_i+\tau\lambda\psi^{-1}\nabla\psi(R_i)+(2\tau\lambda)^{1/2}\chi_i, \tag{9}$$

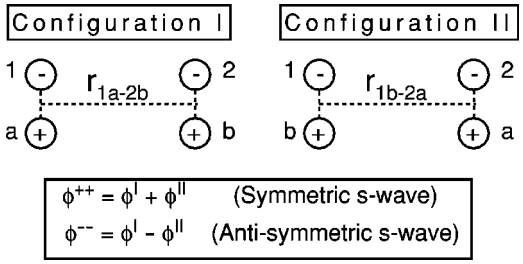

FIG. 1. The two contributions to the exciton scattering wave functions ϕ, at large exciton-exciton separation. The asymptotic form of the s-wave scattering states are symmetric (ϕ^{++}) or antisymmetric (ϕ^{--}) combinations of these configurations. This symmetric/antisymmetric form is used for the trial wave functions f^{++} and f^{--}, using f^I, and f^{II} from Eq. (13).

where χ_i is a normally distributed random variate with zero mean and unit variance and τ is the time step. In the limit of small τ, Eq. (9) describes a process for sampling $\psi^2(R)$.

The matrix element of e^{-tH} is estimated by integrating the local energy of the guiding function $E_{L\psi}(R)=\psi^{-1}(R)H\psi(R)$, along the random walk,

$$W_{n,n+k}=\exp\left\{-\tau\sum_{j=n}^{n+k-1}\tfrac{1}{2}[E_{L\psi}(R_j)+E_{L\psi}(R_{j+1})]\right\}. \tag{10}$$

The estimators for matrices N and H are

$$n_{\alpha\beta}(k\tau)=\frac{1}{p}\sum_{i=1}^{p}F_\alpha^*(R_i)W_{i,i+k}F_\beta(R_{i+k}), \tag{11}$$

$$h_{\alpha\beta}(k\tau)=\frac{1}{p}\sum_{i=1}^{p}F_\alpha^*(R_i)W_{i,i+k}F_\beta(R_{i+k})E_{L\beta}(R_{i+k}), \tag{12}$$

where $F_\alpha=f_\alpha/\psi$ and $E_{L\beta}=f_\beta^{-1}(R)Hf_\beta(R)$ are the local energies of the trial basis states.

C. Form of exciton-exciton scattering wave functions

We now discuss the form for the exciton scattering functions f_α^{++} and f_α^{--}. As mentioned before, interexciton exchange of particles complicates the definition of exciton-exciton separation. There are two configurations for well-separated excitons, as shown in Fig. 1. Configuration I has the electrons and the holes paired as $1a,2b$; and configuration II as $1b,2a$. We choose wave functions $f_\alpha^{\rm I}$ and $f_\alpha^{\rm II}$ to represent these states,

$$f_\alpha^{\rm I}=e^{-\gamma r_{1a}}e^{-\gamma r_{2b}}U_\alpha(r_{1a-2b})\exp\left\{\frac{c_fr_{12}}{1+d_fr_{12}}+\frac{c_gr_{ab}}{1+d_gr_{ab}}-\frac{c_hr_{1b}}{1+d_hr_{1b}}-\frac{c_hr_{2a}}{1+d_hr_{2a}}\right\},$$

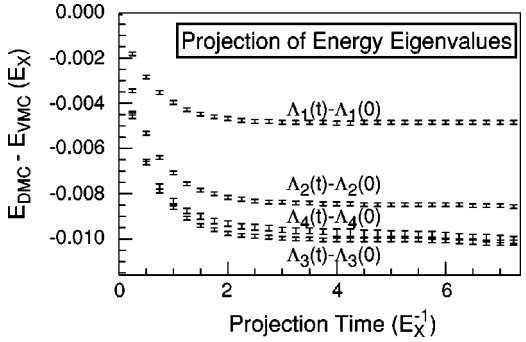

FIG. 2. Change in the projected energy eigenvalues $\Lambda_\alpha(t)-\Lambda_\alpha(0)$ of the DMC states relative to the VMC states as a function of DMC projection time t, for basis states $\alpha=1,2,3,4$. The eigenvalue equation is given by Eqs. (6)–(8), where the Hamiltonian and overlap matrices have been sampled using Eqs. (11) and (12).

$$f_\alpha^{\mathrm{II}}=e^{-\gamma r_{1b}}e^{-\gamma r_{2a}}U_\alpha(r_{1b-2a})\exp\left\{\frac{c_f r_{12}}{1+d_f r_{12}}+\frac{c_g r_{ab}}{1+d_g r_{ab}}-\frac{c_h r_{1a}}{1+d_h r_{1a}}-\frac{c_h r_{2b}}{1+d_h r_{2b}}\right\}, \tag{13}$$

where γ, c_f, d_f, c_g, d_g, c_h, d_h, and parameters in the function $U_\alpha(r)$ are variational. These wave functions represent two excitons in a relative s-wave state. Since these are not eigenstates of the exchange operator for electrons $\hat{P}_e$ or holes $\hat{P}_h$, we take linear combinations of the two for our trial wave functions, $f_\alpha^{++}=f_\alpha^{\mathrm{I}}+f_\alpha^{\mathrm{II}}$ and $f_\alpha^{--}=f_\alpha^{\mathrm{I}}-f_\alpha^{\mathrm{II}}$. For large separation of excitons, the exponential factors prohibit both configurations from simultaneously contributing to the wave function. Thus, a node can be approximated in the scattering wave function by simply requiring that $U_\alpha(r)$ be zero for all $r>R_n$. The error introduced by this approximation is of order $\exp(-2\alpha R_n)$, and is another limit on the use of small values for R_n. Since we only do calculations for low energy scattering and large R_n, the lack of a well-defined exciton-exciton separation distance for short distances does not matter.

This method for calculating scattering properties is very sensitive to the energy spectra $\{E_\alpha(R_n)\}$. To get accurate energies, we do not try to construct and optimize elaborate variational wave functions, but rather use DMC to project the energy from trial wave functions of the form given in Eq. (13). The coefficients γ, c_f, c_g, and c_h are chosen to obey most of the cusp conditions on the wave function for small particle separations. The s-wave envelope functions $U_\alpha(r)$ are taken as solutions to an empirical exciton-exciton scattering potentials,

$$V(r)=\begin{cases}-V_0\left(1-\dfrac{3r^2}{4dr^2}\right), & r\leqslant d\\[2ex] -V_0\dfrac{d^6}{4r^6}, & r>d,\end{cases} \tag{14}$$

where V_0 and d have been self-consistently fit to approximate the energy spectrum of the four-particle scattering states. We take the guiding function ψ to have the same form as the f^{++} wave functions with $U_\psi(r)=[ce^{-r^2/8}+\Sigma_\alpha d_\alpha U_\alpha^2(r)]^{1/2}$. The parameters $\{c,d_\alpha\}$ are chosen to bias sampling towards the collision: $\{c=0,d_1=2,d_2=d_3=d_4=1\}$ for ϕ^{++} states and $\{c=2,d_\alpha=1\}$ for ϕ^{--} states. To check for convergence of the energies in DMC, we plot the energy difference, $E_{\mathrm{DMC}}-E_{\mathrm{VMC}}$, as a function of projection time in Fig. 2. We see convergence after a projection time of $3E_x^{-1}$.

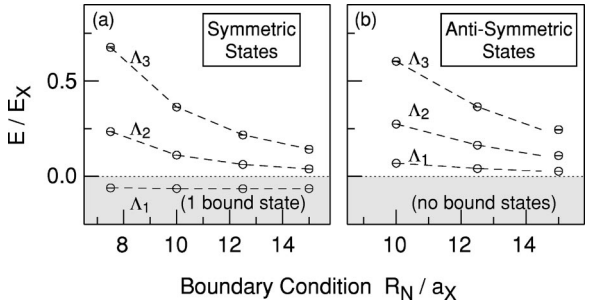

FIG. 3. Energy spectra as a function of nodal position R_N, for (a) symmetric ϕ^{++} states, and (b) antisymmetric ϕ^{--} states, with $m_e=m_h$. The lowest energy curve in (a) is the biexciton with binding energy $E_{\mathrm{B}}=0.0642(3)$. These functions $E(R_N)$ determine the phase shifts δ^{++} and δ^{--}, by the relationship in Eq. (3).

We thus find two energy spectra for each value of R_n as shown in Figs. 3(a) and 3(b). The spectra for the symmetric states ϕ^{++} show a clearly bound biexciton state as seen in Fig. 3(a). The antisymmetric states ϕ^{--}, as shown in Fig. 3(b), have no bound state. The binding energy of the biexciton is $E_{\mathrm{B}}=-0.0642(3)E_x$, in agreement with other ground state calculations, and is insensitive to the position of the node R_N because it is localized. In contrast, the delocalized scattering states are quite sensitive to R_N and their dependence on R_N is a measure of the elastic scattering matrix elements.

D. Calculation of phase shifts

Using Eq. (3), we determine scattering-phase shifts $\delta^{++}(k)$ and $\delta^{--}(k)$, which are shown in Fig. 4 for the equal-mass case. The $k=0$ limits show us that there is one bound symmetric state ϕ^{++} and no bound antisymmetric states ϕ^{--}. The slope at $k=0$ is related to the scattering length a_s by $\delta'(k)=-a_s$. From a cubic polynomial fit to the data, with coefficients given in Table I, we find a

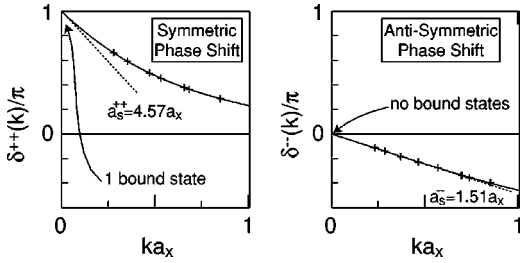

FIG. 4. Phase shifts $\delta(k)$ for the two s-wave scattering states, for $m_e=m_h$, calculated using Eq. (3) and the data from Fig. 3.

TABLE I. Coefficients for polynomomial fit to the low energy part of the phase shift functions for the case $m_e = m_h$.

	c_0	c_1	c_2	c_3
δ^{++}	π	$-4.574(21)$	$2.995(70)$	$-0.829(54)$
δ^{--}	0	$-1.512(29)$	$-0.138(90)$	$0.216(64)$

$=4.57(2)a_x$ for the symmetric state, and $a=1.51(3)$ for the antisymmetric state. These model values are consistent with the measured upper bound $4a_x$ found in Cu_2O.

E. Extracting spin dependence from spatial symmetries

In real semiconductors, electrons and holes can exchange (equivalent to virtual annihilation of the pair), which separates excitons into singlet and triplet energy eigenstates. Although these states are degenerate in our Hamiltonian, the spin-dependent scattering cross sections can be determined for this basis. Due to the antisymmetry of the total wave function, we can infer that states ϕ^{++} and ϕ^{--} have spin eigenstates $|s00\rangle_{eh}$ and $|s11\rangle_{eh}$ where the notation $|ss_e s_h\rangle_{eh}$ stands for total spin s, total electron spin s_e, and total hole spin s_e. We denote the experimentally relevant basis as $|ss_1 s_2\rangle_{ex}$, where the total spin is s, and the spins on the scattering excitons are s_1 and s_2, which take the values 0 for singlet excitons and 1 for triplet excitons. Note that for materials with $j=3/2$ holes (not treated here), the exciton total spin takes the values 1 and 2. Table II lists matrix elements for the change of basis $|ss_e s_h\rangle_{eh} \rightarrow |ss_1 s_2\rangle_{ex}$. Thus, the states $|000\rangle_{eh}$ and $|s11\rangle_{eh}$ act as channels for s-wave exciton-exciton scattering. The matrix elements for scattering through these channels are

$$s^{++}(k) = {}_{eh}\langle 000;k|\hat{s}|000;k\rangle_{eh} = \frac{e^{2i\delta^{++}(k)}-1}{2ik}, \quad (15)$$

TABLE II. Matrix elements for changing spin basis in the two exciton problem. Columns are in the $|s,s_{ee},s_{hh}\rangle_{eh}$ basis and rows are in the ${}_{ex}\langle s,s_{eh},s_{eh}|$ basis.

	$\|000\rangle_{eh}$	$\|011\rangle_{eh}$	$\|101\rangle_{eh}$	$\|110\rangle_{eh}$	$\|111\rangle_{eh}$	$\|211\rangle_{eh}$
${}_{ex}\langle 000\|$	$-\frac{1}{2}$	$\frac{\sqrt{3}}{2}$	0	0	0	0
${}_{ex}\langle 011\|$	$\frac{\sqrt{3}}{2}$	$+\frac{1}{2}$	0	0	0	0
${}_{ex}\langle 101\|$	0	0	$\frac{1}{2}$	$-\frac{1}{2}$	$\frac{\sqrt{2}}{2}$	0
${}_{ex}\langle 110\|$	0	0	$-\frac{1}{2}$	$\frac{1}{2}$	$\frac{\sqrt{2}}{2}$	0
${}_{ex}\langle 111\|$	0	0	$\frac{\sqrt{2}}{2}$	$\frac{\sqrt{2}}{2}$	0	0
${}_{ex}\langle 211\|$	0	0	0	0	0	1

TABLE III. All nonzero s-wave scattering process. Initial and final states are denoted by $|ss_1 s_2\rangle_{ex}$, where s is the total spin and s_1 and s_2 are the individual exciton spins. The coefficients α_+, α_- are for computing the scattering matrix elements, and the coefficients c_{++}, c_{--}, c_{+-} are for computing cross sections. The last column lists the ratio of the scattering length a_s to the exciton radius a_x for the case $m_e = m_h$.

Process	α_+	α_-	c_{++}	c_{--}	c_{+-}	a_s/a_x
$\|000\rangle_{ex} \rightarrow \|000\rangle_{ex}$	$\frac{1}{4}$	$\frac{3}{4}$	$\frac{1}{4}$	$\frac{3}{4}$	$-\frac{3}{16}$	2.128(27)
$\|011\rangle_{ex} \rightarrow \|011\rangle_{ex}$	$\frac{3}{4}$	$\frac{1}{4}$	$\frac{3}{4}$	$\frac{1}{4}$	$-\frac{3}{16}$	3.759(22)
$\|011\rangle_{ex} \rightarrow \|000\rangle_{ex}$	$-\frac{\sqrt{3}}{4}$	$-\frac{\sqrt{3}}{4}$	0	0	$\frac{3}{16}$	$-1.411(17)$
$\|000\rangle_{ex} \rightarrow \|011\rangle_{ex}$	$-\frac{\sqrt{3}}{4}$	$-\frac{\sqrt{3}}{4}$	0	0	$\frac{3}{16}$	$-1.411(17)$
$\|110\rangle_{ex} \rightarrow \|110\rangle_{ex}$	0	$\frac{1}{4}$	0	1	0	0.706(14)
$\|211\rangle_{ex} \rightarrow \|211\rangle_{ex}$	0	1	0	1	0	1.512(29)

$$s^{--}(k) = {}_{eh}\langle S11;k|\hat{s}|S11;k\rangle_{eh} = \frac{e^{2i\delta^{--}(k)}-1}{2ik}. \quad (16)$$

IV. RESULTS

A. Spin dependence of scattering cross sections for the equal mass case

In order to calculate the spin dependence of the scattering matrix elements, we decompose the scattering events into the two channels, $s^{++}(k)$ and $s^{--}(k)$. Using the change of basis matrix, we find $s(k) = \alpha_+ s^{++}(k) + \alpha_- s^{--}(k)$, where the coefficients α_+ and α_- for all nonzero s-wave scattering processes are given in Table III. The s-wave scattering cross sections are given by $\sigma(k) = 8\pi|s(k)|^2$, where there is a factor of 2 enhancement due to the identical particle statistics. For the two channels, the cross sections take the form,

$$\sigma(k) = \frac{8\pi}{k^2}[c_{++}\sin^2\delta^{++} + c_{--}\sin^2\delta^{--} - c_{+-}\sin^2(\delta^{++}-\delta^{--})], \quad (17)$$

where $c_{++} = \alpha_+(\alpha_+ + \alpha_-)$, $c_{--} = \alpha_-(\alpha_+ + \alpha_-)$, and $c_{+-} = \alpha_+\alpha_-$ are tabulated in Table III. The scattering lengths a_s are given by $a_s = -\alpha_+\delta^{++\prime}(0) - \alpha_-\delta^{--\prime}(0)$, where the derivatives of the phase shifts are determined from the linear coefficients in Table I. The scattering lengths for the case $m_e = m_h$ are presented in the last column of Table III.

In Fig. 5 we plot the s-wave scattering cross sections versus scattering momentum for the case $m_e = m_h$ and all nonzero spin configurations. Figure 5(a) shows scattering of two singlet-excitons. Scattering of two triplet-excitons is shown in Fig. 5(b), where the solid line represents the spin aligned $S=2$ state, and the dashed line represents the $S=0$ state. Triplet-triplet scattering is very sensitive to the relative orientation of the exitons, $S=0$, 1, or 2. The $S=0$ state scatters stronger than the $S=2$ state because the $S=0$ state has a large contribution from the s^{++} channel, which is enhanced

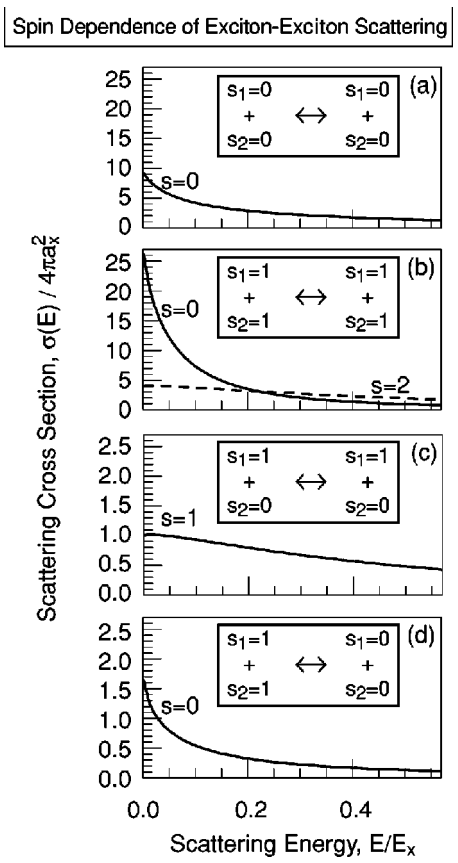

FIG. 5. All nonzero *s*-wave cross sections, Eq. (17), for exciton-exciton scattering with $m_e = m_h$, for the processes: (a) singlet-singlet → singlet-singlet, (b) triplet-triplet → triplet-triplet for total spin $s=0$ (dashed line) and $s=2$ (solid line), (c) triplet-singlet → triplet-singlet with $s=1$, and (d) triplet-triplet → singlet-singlet and singlet-singlet → triplet-triplet, both with $s=0$.

by the weakly bound biexciton. Triplet-excitons in a relative $S=1$ state are spatially antisymmetric and thus have no *s*-wave scattering. We show *s*-wave scattering of triplet-excitons from singlet-excitons in Fig. 5(c). This state has two distinguishable excitons, and can scatter by both *s*-wave and *p*-wave processes (only *s*-wave is treated here). As can be seen in Table III, the only contribution to the cross section is from the weaker s^{--} channel. The coefficient for *s*-wave scattering is particularly small because only half the scattering process is symmetric (*s*-wave), and there is an additional factor of 1/2 that cancels the identical particle factor.

There is also a triplet- to singlet-exciton conversion cross section given in Fig. 5(d). Although this is an inelastic process in experimental situations, it conserves energy according to our model Hamiltonian because we do not have an explicit interband-spin coupling. The conversion of two triplet-excitons to two singlet-excitons can be understood as an inter-exciton exchange of a pair of electrons (or holes). Since the spins of the individual excitons do not correspond to symmetries of the Hamiltonian, they need not remain constant during scattering. This conversion process is a physical consequence of the two inequivalent scattering channels s^{++} and s^{--}. This effect has been reported in experimental[22] and theoretical[6] work on exciton scattering in quantum wells.

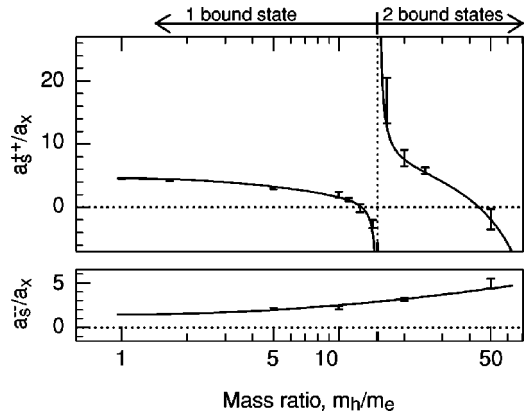

FIG. 6. The scattering lengths a_s^{++} and a_s^{--} as a function of the electron-hole mass ratio. The divergence in a_s^{++} near $m_h/m_e = 15$ is due to the appearance of second bound biexciton state. Solid lines are a guide to the eye.

B. Mass dependence of scattering lengths

The dependence of the cross sections on mass may be numerically studied by our methods. In Fig. 6 we show our calculated a_s^{++} and a_s^{--} as functions of mass ratio, m_h/m_e. We find that the scattering length is remarkably insensitive to the mass ratio for $m_e/m_h < 10$ (corresponding to a wide range of semiconductors), but then diverges near $m_e/m_h = 15$. This feature is lost in previously published theoretical treatments of exciton-exciton scattering. The divergence in a_s^{++} near $m_h/m_e = 15$ is due to the acquisition of a biexciton vibrational state. For $m_e = m_h$ the biexciton has no bound excited states, while a H_2 molecule has 15 bound vibrational states. Our calculations have shown that the first of these appears near $m_h/m_e = 15$, with dramatic effects on the scattering length. The a_s^{--} curve is relatively featureless because there are are no bound antisymmetric states in this range. We interpret the upward drift of a_s^{--} for larger mass ratios as a systematic error due to difficulties in projecting states with large mass difference. The heavy particle determines the projection time ($\sim m^{-1}R^{-2}$), while the light particle determines the diffusion time step τ. The difficulty in handling large mass ratios makes the method (as presented here) complementary to calculations that use the Born-Oppenheimer approximation.

It is important to realize that similar relationships must exist between the scattering length and other material parameters, such as the Luttinger-Kohn parameters describing realistic hole states, external strain, and spin-orbit coupling, to name a few. Theoretical studies of such effects will need similar high-accuracy scattering calculations, but applied to more accurate Hamiltonians, and are an area for future research.

V. CONCLUSION

To summarize, we have shown that there are several significant elastic scattering processes for excitons, and have given numerically exact values for a widely used theoretical model. We find strong triplet-triplet and singlet-singlet scat-

tering, with weaker triplet-singlet scattering and triplet-triplet to singlet-singlet conversion processes. Scattering is relatively insensitive to the mass ratio for $m_h/m_e \lesssim 10$, but becomes very sensitive and actually diverges near $m_h/m_e \approx 15$. DMC has been found to be a good tool for this four-particle excited state calculation, since the detection of weakly bound states requires very accurate evaluation of the correlation energy.

This computational approach should be extended in many ways. The extension to higher angular momentum states would give important corrections at higher scattering energies. Even for low energies, *p*-wave scattering process can be important, and we see no fundamental difficulty of extending this QMC technique to treat *p*-wave scattering. Application to biexciton-biexciton scattering are possible, but would be a bit more difficult because the scattering wave function would then have to describe eight interacting particles.

Most importantly, the method should be adapted to better Hamiltonians so that the sensitivity of the scattering length to material properties for a wide range of materials can be studied. For materials such as Si, Ge, and $In_{1-x}Ga_xAs$, which have $j=3/2$ hole states, a multiband Hamiltonian must be used. To the best of our knowledge, there have been no multiband QMC calcuations on even the ground state exciton and biexciton in these systems. If ground state techniques were developed for those systems, it would be reasonable to extend those techniques to the excited state scattering framework described here. This approach should be quite useful for quantum well and other nanostructure problems. Strain reduces the degeneracy of the valence band edge, so that even materials with a $j=3/2$ hole state in the bulk may be modeled with a single band. Additonally, nanostructures have many more experimental parameters that can affect exciton-exciton interaction, which could be studied by the same bulk techniques described here.

ACKNOWLEDGMENTS

We would like to thank K. O'Hara and J. Carlson for useful discussions. This work was supported by NSF Grants No. ECS 95-09751, No. DMR 98-02373, and No. NSF DGE 93-54978, computer resources at NCSA, and the Department of Physics at the University of Illinois Urbana-Champaign.

*Present address: National Renewable Energy Laboratory, Golden, CO 80401. Email address: jshumway@nrel.gov

[1] D.W. Snoke, J.P. Wolfe, and A. Mysyrowicz, Phys. Rev. B **41**, 11 171 (1990).
[2] D.W. Snoke, D. Braun, and M. Cardona, Phys. Rev. B **44**, 2991 (1991).
[3] H. Haug, Z. Phys. B **24**, 351 (1976).
[4] S.G. Elkomoss and G. Munschy, J. Phys. Chem. Solids **42**, 1 (1981).
[5] S.G. Elkomoss and G. Munschy, J. Phys. Chem. Solids **45**, 345 (1981).
[6] C. Ciuti, V. Savona, C. Piermarocchi, A. Quattropani, and P. Schwendimann, Phys. Rev. B **58**, 7926 (1998).
[7] T.S. Koh, Y.P. Feng, and H.N. Spector, Phys. Rev. B **55**, 9271 (1997).
[8] H.N. Cam, Phys. Rev. B **55**, 10 487 (1997).
[9] L.V. Keldysh and Z.N. Kozlov, Zh. Éksp. Teor. Fiz **53**(3), 978 (1968) [Sov. Phys. JETP **27**, 521 (1997)].
[10] H. Haug and E. Hanamura, Phys. Rev. B **11**, 3317 (1975).
[11] For example, the location of the scattering length divergence at $m_e/m_h \approx 15$, reported later in this paper, is extremely sensitive to an accurate treatment of correlation energy, since it relies on the appearance of a second, weakly bound biexciton state at that mass ratio.
[12] A. Quattropani and J. J. Forney, Nuovo Cimento B **39**, 569 (1977).
[13] E.A. Hyllerass and A. Ore, Phys. Rev. **71**, 43 (1947).
[14] W.F. Brinkman, T.M. Rice, and B. Bell, Phys. Rev. B **8**, 1570 (1973).
[15] M.A. Lee, P. Vashishta, and R.K. Kalia, Phys. Rev. Lett. **51**, 2422 (1983).
[16] D. Bressanini, M. Mella, and G. Morosi, Phys. Rev. A **55**, 200 (1997).
[17] J. Carlson, V.R. Pandharipande, and R.B. Wiringa, Nucl. Phys. A **424**, 47 (1984).
[18] Y. Alhassid and S. E. Koonin, Ann. Phys. **155**, 108 (1984).
[19] J. Carlson and R. Shiavilla, Rev. Mod. Phys. **70**, 743 (1998).
[20] J. Carlson (private communication).
[21] D.M. Ceperley and B. Bernu, J. Chem. Phys. **89**, 6316 (1988).
[22] T. Amand, D. Robart, X. Marie, M. Brousseau, P. Le Jeune, and J. Barrau, Phys. Rev. B **55**, 9880 (1997).